

**Air kerma measurements with Landauer nanoDots  
in Cs-137 and Co-60 beams  
Part I – SSDL exposures free in air**

*A technical document series for CERAD and DoReMi partners  
on the use of nanoDots at FIGARO.*



**Reference:**

E. Lindbo Hansen, P. O. Hetland. Air kerma measurements with Landauer nanoDots in Cs-137 and Co-60 beams. Teknisk dokument nr. 8. Østerås: Norwegian Radiation Protection Authority, 2017. Language: English.

**Key words:**

Dosimetry. Gamma radiation. Air kerma rates. Ionization chambers. Landauer nanoDots. Traceability.

**Abstract:**

This report concerns air kerma in air measurements with Landauer nanoDots (Landauer, Inc., Greenwood, IL) in Cs-137 and Co-60 beams. It establishes through measurements and simulations that nanoDots require additional beam energy appropriate buildup for air kerma in air measurements at these beam qualities.

**Referanse:**

E. Lindbo Hansen, P. O. Hetland. Air kerma measurements with Landauer nanoDots in Cs-137 and Co-60 beams. Teknisk dokument nr. 8. Østerås: Norwegian Radiation Protection Authority, 2017. Språk: Engelsk.

**Emneord:**

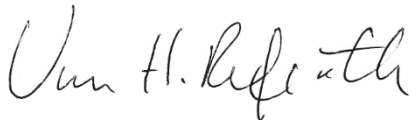
Dosimetri. Gamma-stråling. Luftkermarater. Ionisasjonskamre. Landauer nanoDots. Sporbarhet.

**Resymé:**

Rapporten omhandler målinger av luftkerma i luft med Landauer nanoDots (Landauer, Inc., Greenwood, IL) i Cs-137 og Co-60 felt. Den etablerer gjennom målinger og simuleringer at nanoDots trenger ekstra, energi-tilpasset buildup for målinger av luftkerma i luft ved disse strålingskvalitetene.

Prosjektleder: Åste Søyvik.

Godkjent:



Refseth Unn Hilde, avdelingsdirektør, avdeling overvåkning og forskning

22 sider.

Publisert 2017-12-07.

Statens strålevern, Postboks 55, No-1332 Østerås, Norge.

Telefon 67 16 25 00, faks 67 14 74 07.

E-post: nrpa@nrpa.no

www.nrpa.no

ISSN 2387-5240 (online)

# **Air kerma measurements with Landauer nanoDots in Cs-137 and Co-60 beams**

## ***Part I – SSDL exposures free in air***

A technical document series for CERAD and DoReMi partners on the use of nanoDots at FIGARO.

Report and analysis: Elisabeth Lindbo Hansen (elisabeth.hansen@nrpa.no)

Measurements: Elisabeth Lindbo Hansen, Per Otto Hetland

---

# Contents

---

<b>Air kerma measurements with Landauer nanoDots</b>	<b>1</b>
in Cs-137 and Co-60 beams	1
<i>Part I – SSDL exposures free in air</i>	<b>1</b>
<b>1 Introduction</b>	<b>3</b>
<b>2 Summary of results</b>	<b>3</b>
<b>3 Theory and background</b>	<b>4</b>
3.1 The mass attenuation, mass energy-transfer and mass energy-absorption coefficients, the kerma and the absorbed dose	4
3.2 CSDA ranges of Compton edge electrons in air, C-552, water and PMMA	5
3.3 Cavity theory	6
3.4 Uncertainty	6
<b>4 Materials and methods</b>	<b>7</b>
4.1 Beams	7
4.2 The ionization chambers	8
4.3 Landauer nanoDots and the microStar reader	8
4.4 Physical properties of nanoDots	9
4.5 A Geant4 model of the nanoDot exposures	9
<b>5 Results and discussion</b>	<b>11</b>
5.1 Air kerma rates in the Cs-137 and Co-60 beams	11
5.2 Ratio of the dose on nanoDots to the air kerma	11
5.3 Simulated specific energy imparted to nanoDots as a function of added buildup and backscatter material and field size	13
5.4 Discussion	17
5.5 Comparing the simulations and measurements	17
<b>6 Recommendations and outlook</b>	<b>18</b>
6.1 Buildup for air kerma in air measurements with nanoDots	18
<b>7 Appendix</b>	<b>19</b>
7.1 Cs-137 air kerma in air calibration certificate purchased from Landauer	19
7.2 Exposures of nanoDots with beam energy appropriate buildup at FIGARO for the DoReMi CloGiGat project	20
<b>8 Acknowledgements</b>	<b>20</b>
<b>9 References</b>	<b>21</b>

---

## 1 Introduction

This report concerns air kerma in air measurements with Landauer nanoDots (Landauer, Inc., Greenwood, IL) in Cs-137 and Co-60 beams. Exposures of nanoDots to known air kerma rates in Cs-137 and Co-60 beams were conducted at the Secondary Standard Dosimetry Laboratory (SSDL) at the Norwegian Radiation Protection Authority (NRPA) in May, 2015. The nanoDot detectors and microStar reader are commercially available from Landauer. The technology is based on optically stimulated luminescence (OSL) dosimetry, which is a solid state dosimetry method wherein an insulator or semiconductor that has been irradiated with ionizing radiation emits light upon being irradiated with light. The nanoDot detectors and microStar reader were purchased by the CERAD Center of Excellence in Environmental Radioactivity in 2015 for use at the FIGARO low dose Co-60 irradiation facility.

This report establishes through measurements and simulations that air kerma measurements in air with Landauer nanoDots should be conducted with beam energy appropriate buildup, both in Cs-137 and definitely in Co-60 beams. This applies also to air kerma in air calibration exposures at these beam qualities. The dosimetric capabilities of the nanoDots and microStar reader at FIGARO have been demonstrated for the DoReMi CloGiGat project (see appendix) and will be further documented through future work.

## 2 Summary of results

Cs-137 and Co-60 beams at the SSDL at the NRPA were used to expose nanoDots free in air for various time intervals to air kerma rates that were known from measurements free in air with ionization chambers traceable to the Bureau International des Poids et Mesures (BIPM) [1, 2]. In the circular Cs-137 beam, ionization chambers or nanoDots were placed on the central field axis free in air 2.0 m from the source focus where the field diameter was about 44 cm. In the square Co-60 beam, ionization chambers or nanoDots were placed on the central field axis free in air 6.0 m from the source focus where the field size was roughly 60 cm × 60 cm. In the Cs-137 beam, the air kerma rate in air at the location of the nanoDots was 17.27(0.17) mGy/h and in the Co-60 beam the air kerma rate was 1.465(0.015) Gy/h<sup>1</sup>. So-called “screened” nanoDots were exposed in the beams to an integrated air kerma in the range from approximately 10 mGy to 160 mGy. Following the exposures, nanoDot readouts employed a linear calibration curve for the read dose that was obtained on the Landauer microStar by reading off calibration nanoDots provided by Landauer. Landauer had previously reported that the calibration nanoDots had been exposed free in air without buildup to known air kerma rates in a Cs-137 beam, and that the calibration was assumed to also be appropriate for measurements of air kerma with nanoDots placed free in air without

---

<sup>1</sup> The numbers in parentheses are numerical values for the combined standard uncertainty, given in the units of the quoted results – a notation that is used throughout this report.

---

buildup in a Co-60 beam. The calibration certificate for the calibration nanoDots can be found in the appendix.

For nanoDots exposed free in air without buildup in the Cs-137 beam, the mean ratio of the read dose to the air kerma in air was 96.7(0.4)%. For nanoDots exposed free in air without buildup in the Co-60 beam, this mean ratio was 70.7(0.3)%. The ratio of these mean ratios is 73.2(0.4)%. This means the absorbed dose to nanoDots for a given air kerma in the Co-60 beam was on average 73.2(0.4)% of the absorbed dose to nanoDots in the Cs-137 beam at the same air kerma. Because nanoDots experienced different buildup from air and from electrons liberated in the source and source housing in the two exposures, this ratio is not generally true.

A Geant4 [3-5] model of nanoDot exposures was therefore built to investigate the contribution from secondary electrons to the specific energy imparted to nanoDots as a function of added buildup and backscatter material and field size. The simulations show that modelled nanoDots exposed free in air without buildup in Cs-137 and Co-60 beams can receive a substantial signal originating from secondary electrons liberated in air that varies with the field size and source-to-surface distance unless both are sufficiently large to ensure full buildup. Air kerma measurements in air with Landauer nanoDots should therefore be conducted with beam energy appropriate buildup, both in Cs-137 and definitely in Co-60 beams so that the signal on the nanoDots originates solely from electrons that were liberated either in the buildup or in the materials of the detectors themselves. This applies also to air kerma in air calibration exposures.

## 3 Theory and background

### 3.1 The mass attenuation, mass energy-transfer and mass energy-absorption coefficients, the kerma and the absorbed dose

When photons propagate through matter, energy is transferred from the photon field to matter by electromagnetic interactions. The mass attenuation coefficient  $\mu/\rho$  quantifies through the relation

$$\Phi = \Phi_0 \exp(-(\mu/\rho)x), \quad (1)$$

how much a primary monoenergetic photon fluence  $\Phi_0$  is attenuated by traversing a material of mass thickness  $x = \rho d$  [6]. Here  $\rho$  is the material density and  $d$  the thickness. This attenuation occurs when interactions such as photoelectric absorption, coherent or incoherent scattering and pair production remove photons from the primary field. The mass energy-transfer coefficient  $\mu_{tr}/\rho$  quantifies through the relation

$$K = \Phi \cdot E \cdot (\mu_{tr}/\rho), \quad (2)$$

how much of the monoenergetic photon energy fluence  $\Psi = \Phi \cdot E$  at a point that is on average transferred from the photon field to matter [6]. Here  $E$  is the photon energy and  $K$  the kerma, short for kinetic energy

---

released in matter or kinetic energy released per mass. As the released charged particles travel through matter, some of their initial kinetic energy is transferred back to the photon field as photons of different energies, through processes such as bremsstrahlung, or through fluorescence from excited states in their tracks. This fraction is quantified through the factor  $g$ . The product

$$\mu_{en}/\rho = \mu_{tr}/\rho \cdot (1 - g), \quad (3)$$

is known as the mass energy-absorption coefficient [6]. The mass energy-absorption coefficient quantifies how much of the kerma that remains as energy deposited in matter once all secondary and later generations of particles have come to rest and fluorescence losses in their tracks have been accounted for. The average energy deposited in matter per mass of matter is known as the absorbed dose  $D$  [7]. The air kerma free in air and the absorbed dose to water at certain depths in water are the quantities which primary and secondary standard dosimetry laboratories (PSDLs and SSDLs) normally provide calibrations for in Cs-137 and Co-60 beams [8].

### 3.2 CSDA ranges of Compton edge electrons in air, C-552, water and PMMA

For photons of energies around 1 MeV, the most common interaction between the photon field and matter is Compton scattering [9], which leads to the liberation of secondary electrons and scattered photons. The kinetic energy of the electrons is subsequently deposited as tracks of ionizations and excitations in matter. The continuous-slowing-down approximation (CSDA) range is a close approximation to the average path length that the electrons travel as they slow down to rest [10]. The projected range is shorter than the CSDA range because the electrons do not travel in straight lines.

For Cs-137 gamma rays at 662 keV, the maximum energy of secondary electrons originating from Compton events is 478 keV [11]. For Co-60 gamma rays at 1.17 and 1.33 MeV, the maximum energy of such electrons is respectively 960 keV and 1.12 MeV [11]. Table 1 below shows interpolated CSDA ranges and approximate path lengths for electrons at these energies in dry air, in C-552 air-equivalent plastic, in water and in poly(methyl methacrylate) (PMMA).

*Table 1: The linearly interpolated CSDA range and approximate path length of electrons of different kinetic energies in dry air, in C-552 air-equivalent plastic, in water and in PMMA, based on tabulated data from NIST [10].*

Material	Density	Mean excitation energy	Kinetic energy of electrons	Interpolated CSDA range	Path length
	[g/cm <sup>3</sup> ]	[eV]	[MeV]	[g/cm <sup>2</sup> ]	[cm]
Dry air	1.205 · 10 <sup>-3</sup>	85.7	0.478	0.19	1.5 · 10 <sup>2</sup>
			0.960	0.46	3.8 · 10 <sup>2</sup>
			1.12	0.57	4.7 · 10 <sup>2</sup>
C-552	1.760	86.8	0.478	0.19	0.11
			0.960	0.46	0.26
			1.12	0.57	0.33
Water	1.000	75.0	0.478	0.16	0.16
			0.960	0.41	0.41
			1.12	0.50	0.50
PMMA	1.190	74.0	0.478	0.17	0.14
			0.960	0.42	0.36
			1.12	0.52	0.44

### 3.3 Cavity theory

Cavity theory describes how measurements made with detectors can be related to dosimetric quantities in a medium of interest. Cavities are traditionally thought of as thin-walled, thick-walled, small, intermediate or large. Thin-walled, small cavities are basically electron detectors, where the measured signal comes from electrons that were liberated outside of the detector and that cross it [12]. The measured signal on thick-walled cavities on the other hand originates from electrons that were liberated in the wall and materials of the detector [12]. The wall should be sufficiently thick for secondary electrons produced outside of the detector to be stopped completely in the wall [12]. Thick-walled detectors may therefore be thought of as photon detectors. Cavities that are intermediate between these two extremes are traditionally referred to as so-called Burlin cavities [12]. Their signal originates both from secondary electrons that were liberated outside of the detector and from secondary electrons that were liberated in the detector materials.

### 3.4 Uncertainty

Uncertainty involves both sample statistics and the estimation of population parameters. In the following, the sample mean  $\bar{X}$  of  $N$  measures  $X_i$  is calculated as [13]

$$\bar{X} = (1/N) \sum_1^N X_i, \quad (4)$$

and the sample standard deviation  $s_N$  as [13]

$$s_N = \sqrt{(1/N) \sum_1^N (X_i - \bar{X})^2}. \quad (5)$$

If the sample was drawn from a population then the sample estimate for the population mean  $\mu$  is obtained as [13, 14]

$$\hat{\mu} = \bar{X}, \quad (6)$$

and the sample estimate for the population standard deviation  $\sigma$  as [13, 14]

$$\hat{\sigma} = \sqrt{(N/(N-1))} \cdot s_N. \quad (7)$$

According to the central limit theorem, the sample estimate for the population mean is itself a normally distributed random variable with mean  $\hat{\mu}$  and standard deviation  $\hat{\sigma}/\sqrt{N}$  [14]. The result of  $N$  measures  $X_i$  may therefore be found as [14, 15]

$$\hat{\mu} \pm \hat{\sigma}/\sqrt{N}, \quad (8)$$

where  $\hat{\sigma}/\sqrt{N}$  is the standard uncertainty of the sample estimate of the population mean. Following the Guide to the Expression of Uncertainty in Measurement (GUM) [15], we report the mean  $\hat{\mu}$  with the numerical value of the standard uncertainty  $\hat{\sigma}/\sqrt{N}$  indicated in parentheses.

When calculations are involved in arriving at a result, uncertainty propagation rules describe how standard uncertainties are combined to form a combined standard uncertainty of the result. As an example, the difference  $d$  between the means of  $N_1$  measures  $X_{i,1}$  and  $N_2$  measures  $X_{i,2}$  may be found as

$$d = (\hat{\mu}_1 - \hat{\mu}_2) \pm \sqrt{(\hat{\sigma}_1/\sqrt{N_1})^2 + (\hat{\sigma}_2/\sqrt{N_2})^2}, \quad (9)$$

assuming  $X_{i,1}$  and  $X_{i,2}$  are uncorrelated. Similarly, the ratio  $r$  of the means of  $N_1$  measures  $X_{i,1}$  and  $N_2$  measures  $X_{i,2}$  may be found as

$$r = (\hat{\mu}_1/\hat{\mu}_2) \cdot \left( 1 \pm \sqrt{((\hat{\sigma}_1/\sqrt{N_1})/\hat{\mu}_1)^2 + ((\hat{\sigma}_2/\sqrt{N_2})/\hat{\mu}_2)^2} \right), \quad (10)$$

again assuming  $X_{i,1}$  and  $X_{i,2}$  are uncorrelated. As before, we report results from such calculations with the numerical value of the standard uncertainty indicated in parentheses.

## 4 Materials and methods

### 4.1 Beams

Cs-137 and Co-60 beams at the SSDL at the NRPA were used to expose nanoDots free in air without buildup for various time intervals to known air kerma rates. The air kerma at the points of exposure was measured

with ionization chambers traceable to BIPM, as described in the following section. In the circular Cs-137 beam, ionization chambers or nanoDots were placed on the central field axis free in air 2.0 m from the source focus where the field diameter was about 44 cm. In the square Co-60 beam, ionization chambers or nanoDots were placed on the central field axis free in air 6.0 m from the source focus where the field size was roughly 60 cm × 60 cm.

#### 4.2 The ionization chambers

An Exradin A6 ionization chamber (serial number XQ102232) was used for measuring air kerma in air in the Cs-137 beam. The chamber is traceable for measurements of air kerma in a Cs-137 beam to BIPM [1]. From the measured charge  $M$  accumulated over time  $t$ , the air kerma rate is calculated as

$$\dot{K} = (N_K \cdot M \cdot k_\rho) / t. \quad (11)$$

For the Exradin A6, the air kerma calibration factor  $N_K = 37.87(0.08)$  Gy/mC at reference conditions of  $T_0 = 20.0$  °C (293.2 K) and  $P_0 = 101.325$  kPa [1]. The factor  $k_\rho$  provides corrections for deviations in air density from reference conditions. The correction factor is calculated as

$$k_\rho = (T \cdot P_0) / (T_0 \cdot P), \quad (12)$$

where  $(T_0, P_0)$  is the temperature (in K) and pressure at reference conditions and  $(T, P)$  the temperature and pressure at the measurement conditions. For the measurements in the Cs-137 beam, the ambient air pressure was 99.03 kPa, the temperature 21.2 °C (294.4 K) and the relative humidity about 50%. The combined relative standard uncertainty in the determination of  $\dot{K}$  was 0.3% (as reported by the SSDL at the NRPA).

A Capintec PR-06G ionization chamber (serial number 8429) with buildup cap was used for measuring air kerma in air in the Co-60 beam. The chamber with buildup is traceable for measurements of air kerma in a Co-60 beam to BIPM [2]. For the Capintec PR-06G, the air kerma calibration factor  $N_K = 46.09(0.07)$  Gy/μC at reference conditions of  $T_0 = 20.0$  °C (293.2 K) and  $P_0 = 101.325$  kPa [2]. For the measurements in the Co-60 beam, the ambient air pressure was 98.64 kPa, the temperature 21.4 °C (294.6 K) and the relative humidity about 50%. The combined relative standard uncertainty in the determination of  $\dot{K}$  was 0.3% (as reported by the SSDL at the NRPA).

#### 4.3 Landauer nanoDots and the microStar reader

The nanoDot OSL detectors and the microStar reader are commercially available from Landauer (Landauer, Inc., Greenwood, IL). The detectors and reader have been investigated with respects to various properties like dose linearity and angular dependence in different photon and electron beams [16-19], although for many situations, a thorough characterization is lacking. In the current work, newly purchased so-called “screened” nanoDots were first annealed and then exposed to known air kerma rates in the Cs-137 and Co-60 beams. Immediately following annealing, the blank signal on each nanoDot was read off five times, each

---

time with a different holder in order to average over mechanical differences between the holders. For the exposures, nanoDots were glued facing the source onto the center of thin crosses of scotch tape attached to an approximately 40 cm × 40 cm thin cutout cardboard frame. One day after the exposures, the post exposure signal was read off five times with the five different holders and the post anneal signal as well as the measured accumulated background since annealing subtracted. All readouts employed a linear calibration curve for the read dose that was obtained on the microStar by reading off calibration nanoDots provided by Landauer. The calibration certificate for the calibration nanoDots can be found in the appendix. Landauer had previously reported that the calibration nanoDots had been exposed free in air without buildup to known air kerma rates in a Cs-137 beam, and that the calibration was assumed to also be appropriate for measurements of the air kerma with nanoDots placed free in air without buildup in a Co-60 beam.

#### **4.4 Physical properties of nanoDots**

The nanoDot casings were measured to have outer dimensions of 10.0 mm × 10.0 mm × 2.0 mm, and to enclose a 0.3 mm thick sensitive detector disk with a diameter of 5.0 mm. A nanoDot was measured to have a mass of 0.1313 g and the sensitive detector disk a mass of 0.0098 g. The casing is made of ABS plastic [17] (molecular formula  $C_{15}H_{17}N$ ) with density 1.03 g/cm<sup>3</sup> [16] and the wall thickness immediately in front of and behind the sensitive detector disk was measured to 0.4 mm. The intrinsic buildup in front of the sensitive detector from the casing is therefore a mass thickness of 0.04 g/cm<sup>2</sup> of ABS. The CSDA range in ABS of the most energetic electrons in a Cs-137 beam is about 0.17 g/cm<sup>2</sup> and in a Co-60 beam about 0.51 g/cm<sup>2</sup> [10], corresponding to path lengths of respectively 0.16 cm and 0.50 cm. The ABS wall thickness is therefore roughly a factor four too small for providing sufficient buildup for measurements of air kerma in a Cs-137 beam, and a factor thirteen too small for providing sufficient buildup for measurements of air kerma in a Co-60 beam. The sensitive detector disk consists of an Al<sub>2</sub>O<sub>3</sub>:C powder in a polymer binder. Al<sub>2</sub>O<sub>3</sub> has a native density of about 4.0 g/cm<sup>3</sup>, whereas the average density of the whole disk is 1.7 g/cm<sup>3</sup>. The sensitive detector disk therefore has an intrinsic buildup along its full thickness of about 0.05 g/cm<sup>2</sup> of the Al<sub>2</sub>O<sub>3</sub>:C powder and binder, about a factor of ten smaller than the CSDA range of the most energetic Compton electrons in a Co-60 beam.

#### **4.5 A Geant4 model of the nanoDot exposures**

A simplified Geant4 [3-5] model of the nanoDots was built based on information available in the literature [16-19] and on the physical measurements. The nanoDot casings were modelled as hollow boxes with outer dimensions of 10.00 mm × 10.00 mm × 2.00 mm and inner dimensions of 8.00 mm × 8.00 mm × 0.12 mm, consisting of ABS plastic with a density of 1.03 g/cm<sup>3</sup> and a mean excitation energy of 65.401 eV. The hollow inner space was filled with air or galactic vacuum and the sensitive detectors. These were considered as 0.30 mm thick disks with a diameter of 5.00 mm consisting of 50% by mass (0.005 g) of Al<sub>2</sub>O<sub>3</sub> powder and 50% by mass (0.005 g) of a plastic binder assumed to have the same molecular formula

as ABS. The detectors were therefore modelled to consist of a homogenous material with molecular formula of  $\text{Al}_2\text{O}_3 \cdot 2(\text{C}_{15}\text{H}_{17}\text{N})$ , having a mean density of  $1.7 \text{ g/cm}^3$  and a mean excitation energy of  $73.691 \text{ eV}$ . The air inside and surrounding the nanoDots was set to have a density of  $1.299 \cdot 10^{-3} \text{ g/cm}^3$ , which is the density of air at reference conditions with a temperature of  $T_0 = 20.0 \text{ }^\circ\text{C}$  ( $293.2 \text{ K}$ ) and pressure of  $P_0 = 101.325 \text{ kPa}$ . The mean excitation energy of air was  $85.7 \text{ eV}$ . The galactic vacuum had a density of  $1 \cdot 10^{-25} \text{ g/cm}^3$  and a mean excitation energy of  $21.8 \text{ eV}$ . The world was modelled as an  $L \times L \times L$  box of air or galactic vacuum where  $L$  was  $2 \cdot 4 \text{ m}$ . The nanoDots were placed in air or in vacuum at the center of the box. Buildup materials were added as blocks of PMMA with a density of  $1.190 \text{ g/cm}^3$  and a mean excitation energy of  $74.0 \text{ eV}$ , or as blocks of C-552 with a density of  $1.760 \text{ g/cm}^3$  and a mean excitation energy of  $86.8 \text{ eV}$ , placed immediately in front of the nanoDots. A simulation was also run with the buildup being a halfsphere of water with a density of  $1.000 \text{ g/cm}^3$  and a mean excitation energy of  $75.0 \text{ eV}$ , and a radius of  $1.00 \text{ cm}$ . For this configuration, nanoDots were embedded in the surface of the cutout flat side of the halfsphere. This configuration simulates a CIRS plastic water buildup cap for nanoDots (CIRS, Inc., Norfolk, VA). Backscatter materials were added as blocks of water with dimensions of  $1.0 \text{ m} \times 1.0 \text{ m} \times 1.0 \text{ m}$ , placed immediately behind the nanoDots.

The beams were simulated as flat and parallel, originating free in air with an initial photon fluence  $\Phi_0$  at the edge of the world volume, and incident onto the front face of the nanoDots. The primary photon fluence that reaches the location of the nanoDots at  $L/2$  can be written as (see equation (1))

$$\Phi = \Phi_0 \exp(-(\mu/\rho) \cdot \rho \cdot (L/2)), \quad (13)$$

where  $\rho$  is the density and  $\mu/\rho$  the mass attenuation coefficient, which for Cs-137 and Co-60 beams in air is of respectively between  $8.055 \cdot 10^{-2}$  and  $7.074 \cdot 10^{-2} \text{ cm}^2/\text{g}$  (at between  $600$  and  $800 \text{ keV}$ ) and of  $5.687 \cdot 10^{-2} \text{ cm}^2/\text{g}$  (at  $1.25 \text{ MeV}$ ) [6]. Linear interpolation between the data at  $600$  and  $800 \text{ keV}$  gives an estimate for the mass attenuation coefficient at  $662 \text{ keV}$  of  $7.751 \cdot 10^{-2} \text{ cm}^2/\text{g}$ .

The simulations were performed with the G4EmStandardPhysics\_option4 physics list. The mean specific energy imparted to nanoDots was tallied from between ten and fifteen repeated runs and the results normalized to an initial photon fluence of  $\Phi_0 = 1 \cdot 10^6 \text{ 1/cm}^2$ . The simulated ratio  $r$  of the specific energy imparted to the nanoDots  $S$  to the air kerma  $K$  from the primary photon beam free in air at the location of the nanoDots can be found as

$$r = S/K = S/(\Phi \cdot E \cdot \mu_{tr}/\rho), \quad (14)$$

where  $E$  is the photon energy and  $\mu_{tr}/\rho$  the mass energy-transfer coefficient for air. The mass energy-transfer coefficients were assessed from (see equation (3))

$$\mu_{tr}/\rho = (\mu_{en}/\rho)/(1 - g), \quad (15)$$

where  $\mu_{en}/\rho$  is the mass energy-absorption coefficient and  $g$  accounts for the fraction of the initially transferred energy that escapes as photons. The mass energy-absorption coefficients for Cs-137 and Co-60

---

beams in air are of respectively between  $2.953 \cdot 10^{-2}$  and  $2.882 \cdot 10^{-2}$   $\text{cm}^2/\text{g}$  (at between 600 and 800 keV) and of  $2.666 \cdot 10^{-2}$   $\text{cm}^2/\text{g}$  (at 1.25 MeV) [6]. Linear interpolation between the data at 600 and 800 keV gives an estimate for the mass energy-absorption coefficient at 662 keV of  $2.931 \cdot 10^{-2}$   $\text{cm}^2/\text{g}$ . It was assumed that in a Cs-137 beam  $g = 0.0012$  and in a Co-60 beam  $g = 0.0032$ .

## 5 Results and discussion

### 5.1 Air kerma rates in the Cs-137 and Co-60 beams

The Exradin A6 and Capintec PR-06G ionization chambers were used to measure air kerma rates in air in respectively the Cs-137 and Co-60 beams. The relative standard uncertainty on the measured air kerma rates was 0.3% in both beams, whereas the relative standard uncertainty on the air kerma rates at the location of the nanoDots was estimated to 1.0 %. The additional uncertainty arises from imprecision in the positioning of nanoDots. It was thus found that in the circular Cs-137 beam, the air kerma rate at the location of the nanoDots 2.0 m from the source focus was  $17.27(0.17)$  mGy/h. In the square Co-60 beam, the air kerma rate at the location of the nanoDots 6.0 m from the source focus was  $1.465(0.015)$  Gy/h. Note that because the ionization chambers are thick-walled cavities in the Cs-137 and Co-60 beams [8], they are sensitive to the photon fluence that strikes them and ideally insensitive to secondary electrons resulting from buildup in air or in the materials of the source and source housing.

### 5.2 Ratio of the read dose on nanoDots to the air kerma

Tables 1 and 2 show the ratio of the background corrected measured read dose on the nanoDots to the air kerma to which they had been exposed. For nanoDots exposed in the Cs-137 beam, the mean ratio of the read dose to the air kerma in air was  $96.7(0.4)\%$ . For nanoDots exposed in the Co-60 beam, this mean ratio was  $70.7(0.3)\%$ . The ratio of these mean ratios is  $73.2(0.4)\%$ . This means the absorbed dose to nanoDots for a given air kerma in the Co-60 beam was on average  $73.2(0.4)\%$  of the absorbed dose to nanoDots in the Cs-137 beam at the same air kerma. However, because nanoDots experienced different buildup from air and from the materials of the source and source housing in the two exposures, this ratio is not generally true. To investigate the contribution from secondary electrons liberated in air to the absorbed dose to the sensitive detector disks, the next section presents results from Geant4 [3-5] simulations of nanoDot exposures.

Table 2: The air kerma in air at the location of nanoDots in the Cs-137 beam, the background corrected measured dose read on the nanoDots and the ratio of this value to the air kerma. The uncertainty is the combined standard uncertainty, obtained from a Type A statistical evaluation for the background corrected read dose. The mean ratio of the read dose to the air kerma is 0.967(0.004) (see equation (8)).

Air kerma in air at the location of nanoDots	Background corrected read dose on nanoDots	Ratio of read dose to air kerma
[mGy]	[mGy]	[1]
0	0.000(0.011)	
10.0(0.1)	9.72(0.15)	0.971(0.018)
10.0(0.1)	9.73(0.15)	0.972(0.018)
40.0(0.4)	38.7(0.5)	0.967(0.016)
40.0(0.4)	38.3(0.4)	0.957(0.014)

Table 3: The air kerma in air at the location of nanoDots in the Co-60 beam, the background corrected measured dose read on the nanoDots and the ratio of this value to the air kerma. The uncertainty is the combined standard uncertainty, obtained from a Type A statistical evaluation for the background corrected read dose. The mean ratio of the read dose to the air kerma is 0.707(0.003) (see equation (8)).

Air kerma in air at the location of nanoDots	Background corrected read dose on nanoDots	Ratio of read dose to air kerma
[mGy]	[mGy]	[1]
0	0.000(0.013)	
10.3(0.1)	7.39(0.10)	0.721(0.012)
10.3(0.1)	7.23(0.12)	0.706(0.014)
20.3(0.2)	14.2(0.3)	0.702(0.015)
40.3(0.4)	28.0(0.5)	0.696(0.014)
40.3(0.4)	28.5(0.4)	0.707(0.013)
80.3(0.8)	56.7(0.8)	0.706(0.013)
160.2(1.6)	114.0(1.8)	0.712(0.013)
160.2(1.6)	113.5(1.6)	0.709(0.012)

---

### 5.3 Simulated specific energy imparted to nanoDots as a function of added buildup and backscatter material and field size

Figures 1, 2 and 3 show results from Geant4 [3-5] simulations of nanoDot exposures. When the modelled nanoDots are exposed free in air to Cs-137 and Co-60 beams of increasing cross sectional areas (Figure 1) the specific energy imparted increases: in the Cs-137 beam from 80.5(0.9)% of the air kerma free in air at a beam size of 1.0 cm × 1.0 cm to about 105 % of the air kerma for beams larger than 40.0 cm × 40.0 cm; and in the Co-60 beam from 34.7(0.3)% of the air kerma free in air at a beam size of 1.0 cm × 1.0 cm to about 106 % of the air kerma for beams larger than 200.0 cm × 200.0 cm.

When nanoDots are exposed with buildup in vacuum to Co-60 beams with cross-sections that cover their surface area (Figure 2), the specific energy imparted initially increases as the buildup thickness increases because more secondary electrons become available and then decreases because of attenuation. In the case of C-552 buildup, the simulated specific energy imparted reaches a maximum for a buildup thickness of 0.250 cm, where the ratio of the specific energy imparted to the air kerma at the location of the nanoDots is respectively 101.5(0.8)% or 104.0(0.8)%, depending on whether the calculation of the air kerma does not or does take into account attenuation through the buildup (Figure 3). With PMMA buildup, the maximum is reached for a buildup thickness of 0.325 cm, where the ratio of the specific energy imparted to the air kerma at the location of the nanoDots is respectively 104.2(0.6)% or 107.0(0.6)%, again depending on whether the calculation of the air kerma does not or does take into account attenuation through the buildup (Figure 3). Because the only commercially available buildup for nanoDots suitable for Co-60 beams is CIRS plastic water caps (with the smallest available radius being 1.0 cm), Figure 3 also shows the results of simulations where the buildup was such a modelled halfsphere of water. In this case, the ratio of the specific energy imparted to the air kerma was respectively 100.5(0.6)% or 107.0(0.6)%. In Figure 3, the simulations with water buildup also show that the addition of a 1.0 m × 1.0 m × 1.0 m backscatter block of water serves to increase the ratio of the specific energy imparted to the air kerma by roughly 4%.

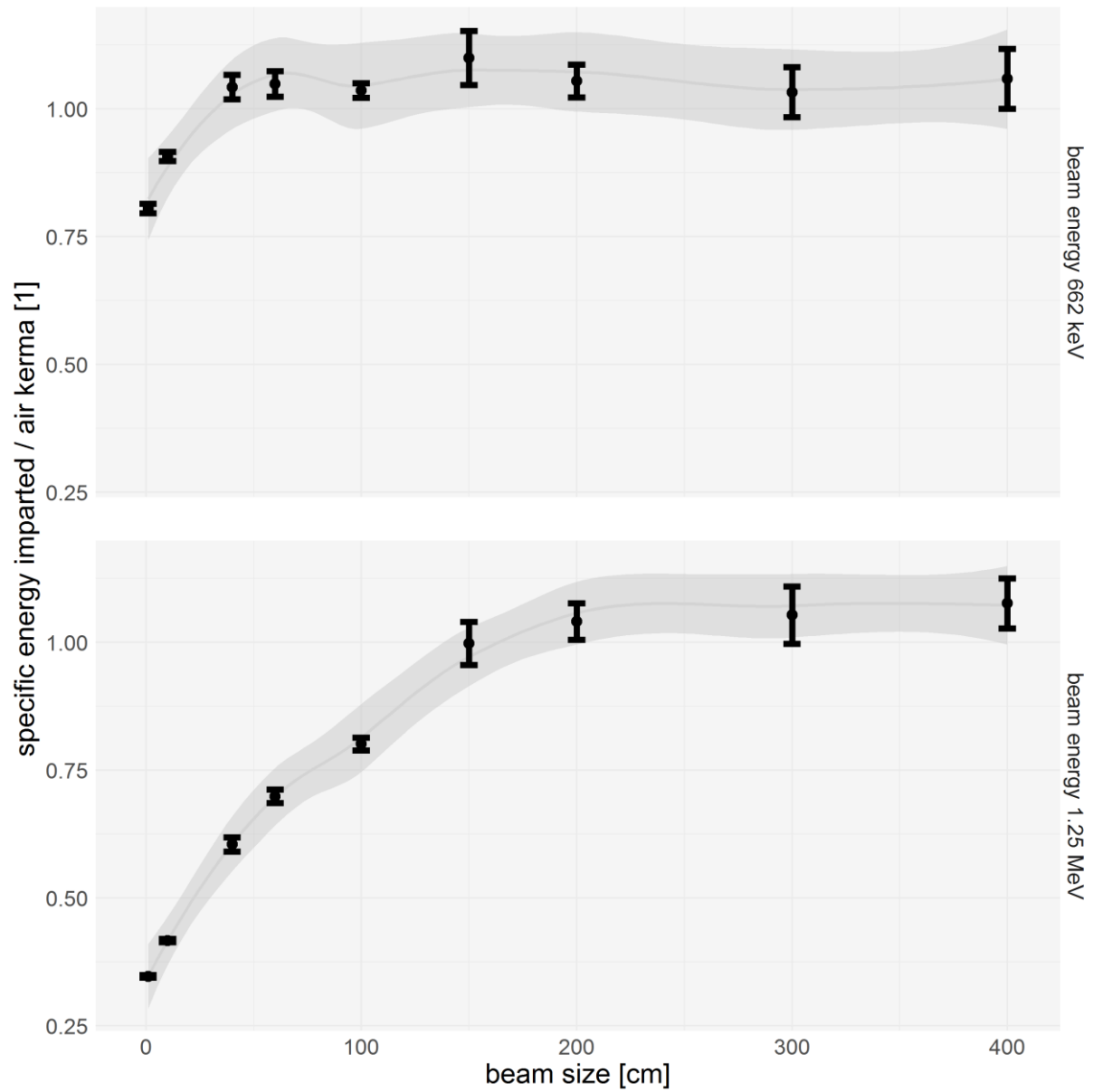


Figure 1: The effect of an increasing beam size on the ratio of the simulated specific energy imparted to the sensitive detector disks to the calculated air kerma at their location free in air. The beams had a square cross-section and the beam size is the size of the sides of the square. The top figure shows data for a Cs-137 beam (at 662 keV) and the bottom figure data for a Co-60 beam (at 1.25 MeV). The grey lines are the loess smoothed regression lines for the data and the grey areas indicate 95% confidence intervals.

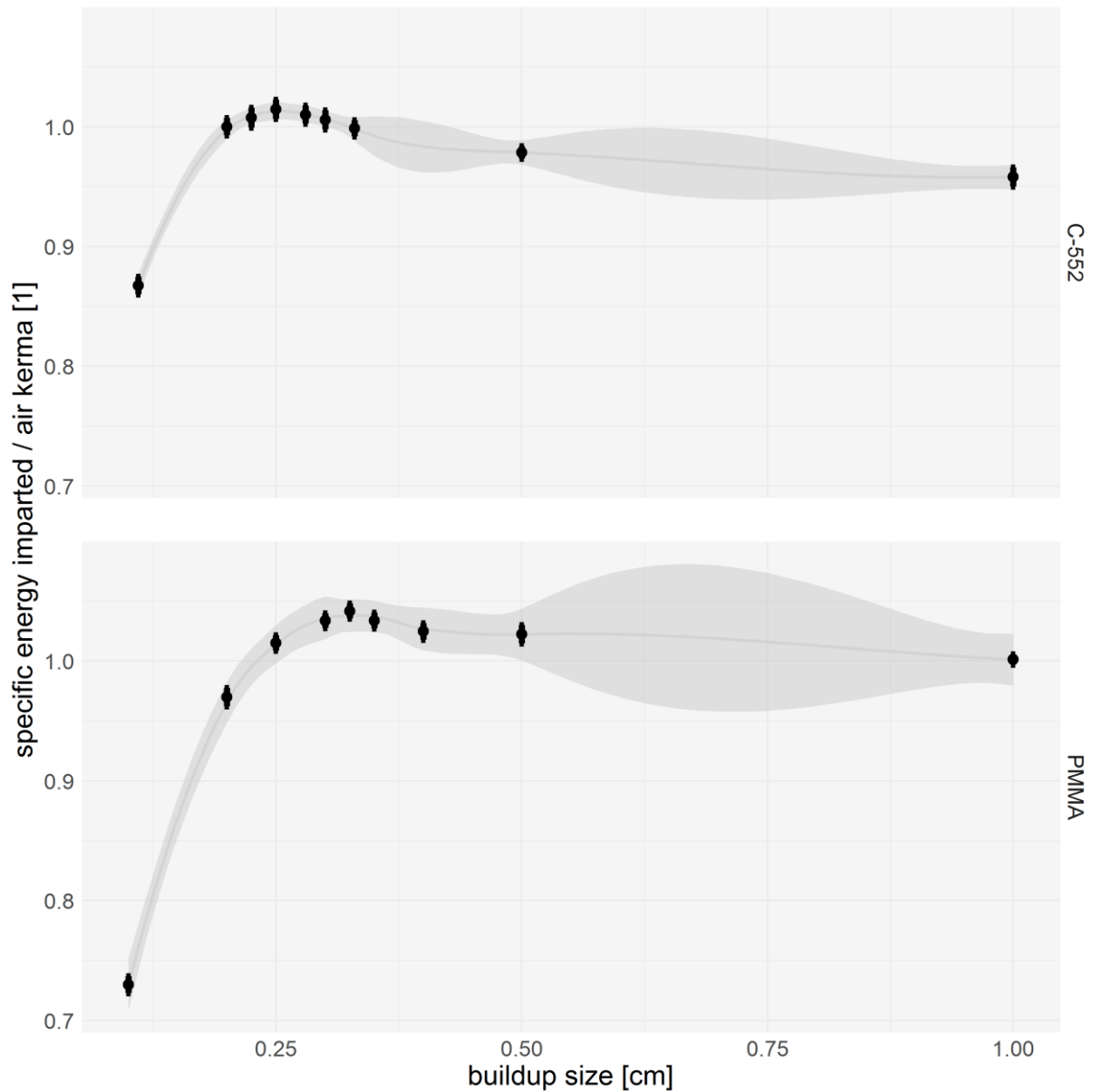


Figure 2: The effect of added C-552 or PMMA buildup on the ratio of the simulated specific energy imparted to the sensitive detector disks in vacuum to the calculated air kerma at their location in a Co-60 beam. The beam size was 10 cm  $\times$  10 cm. The buildup blocks were 2.0 cm  $\times$  2.0 cm  $\times$  z of C-552 (top figure) or PMMA (bottom figure), with z shown on the x-axis. The grey lines are the loess smoothed regression lines for the data and the grey areas indicate 95% confidence intervals. The confidence interval is larger over ranges in the buildup size where there are relatively fewer simulated data points.

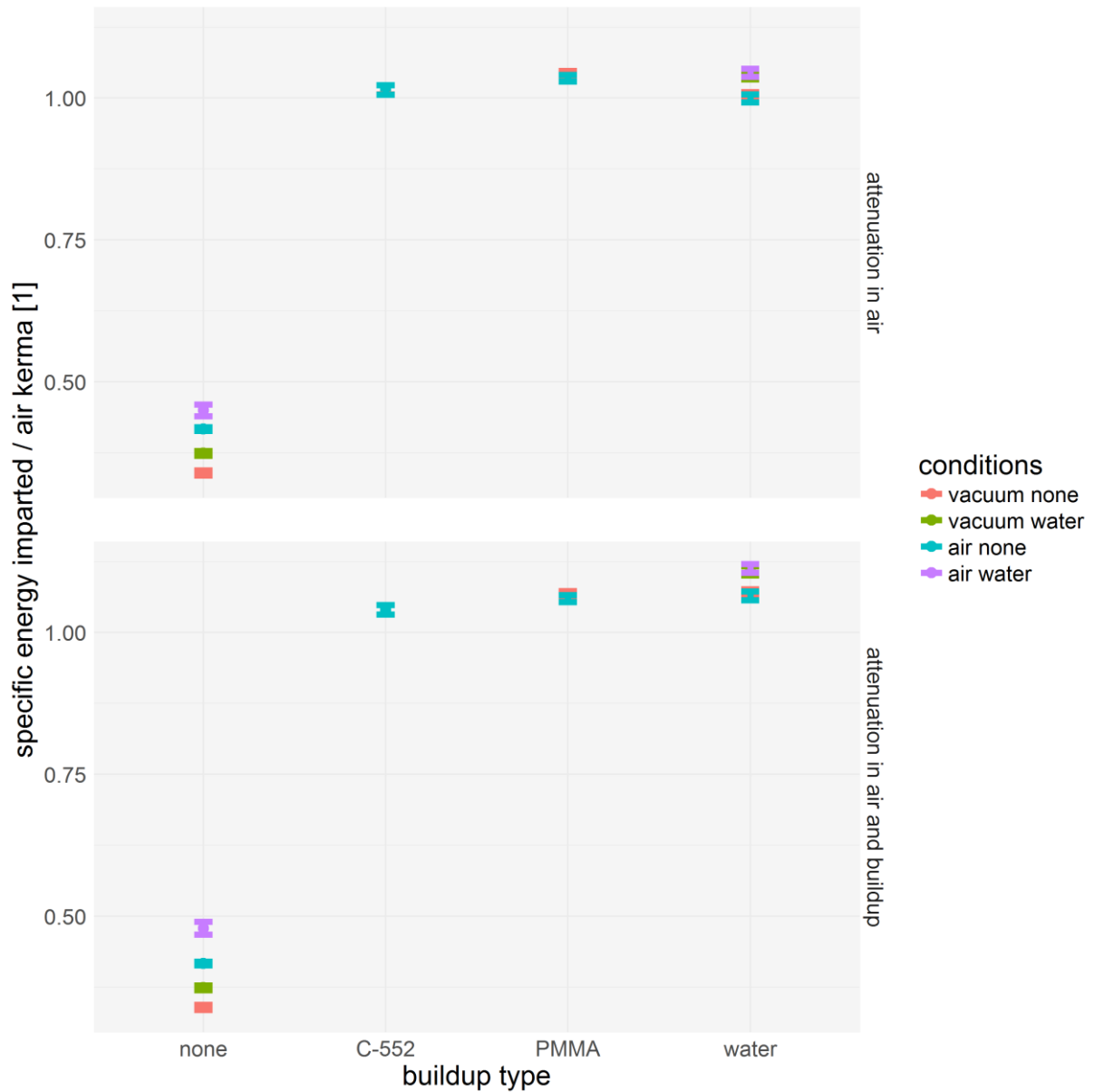


Figure 3: The effect of placing detectors with or without buildup in vacuum or in air and adding backscatter in a Co-60 beam. The beam size was  $10\text{ cm} \times 10\text{ cm}$ . The buildup was blocks consisting of  $2.0\text{ cm} \times 2.0\text{ cm} \times 0.250\text{ cm}$  of C-552 or  $2.0\text{ cm} \times 2.0\text{ cm} \times 0.325\text{ cm}$  of PMMA or a  $1.000\text{ cm}$  in radius halfsphere of water. The backscatter was a  $1.0\text{ m} \times 1.0\text{ m} \times 1.0\text{ m}$  cube of water placed immediately behind the detector. The conditions color coded on the figure denote whether exposures took place in vacuum or air and whether there was no backscatter present or water backscatter. In the case of the buildup being C-552, the data points in vacuum and in air are overlapping. In the topmost figure, the y-axis shows the specific energy imparted divided by the air kerma as it would have been at the location of the nanoDots without any buildup, detector or backscatter materials in the beam (e.g. taking into account only attenuation in air). In the bottom figure, the air kerma in the denominator for the y-axis also took into account attenuation through the full thickness of the buildup.

---

## 5.4 Discussion

The current work demonstrates through measurements and simulations that nanoDots exposed free in air without buildup in Cs-137 and Co-60 beams can receive a substantial signal originating from secondary electrons liberated in air or in the materials of the source and source housing that varies with the field size and source-to-surface distance unless both are sufficiently large to ensure full buildup. The simulations also show that the presence of air in exposures with appropriate buildup and backscatter has a minimal effect on the specific energy imparted to the detectors. This property is necessary when nanoDots calibrated for air kerma in one beam are used for measuring air kerma in another beam with a different field size or source-to-surface distance. The simulations also illustrate how the specific energy imparted to nanoDots is much more sensitive to conditions with too little buildup (determined by the electron range) than too much buildup (determined by the photon linear attenuation coefficient). In other words, the penalty for missing 1 mm of buildup is more severe than the penalty for having 1 mm too much. Finally, this property also serves to emphasize that small inaccuracies in the physical dimensions of simulated nanoDots can have a quite strong effect on simulation outcomes. This is especially true for Cs-137 beams, in which the simulated nanoDots almost have enough intrinsic buildup. For Co-60, the effect of inaccuracies are less severe because of the larger buildup dimensions required.

## 5.5 Comparing the simulations and measurements

The results of the simulations of nanoDot exposures free in air at a field sizes between 60 cm × 60 cm and 100 cm × 100 cm are in general agreement with the measurements, which found that the absorbed dose to nanoDots for a given air kerma in the Co-60 beam was on average 73.2(0.4)% of the absorbed dose to nanoDots in the Cs-137 beam at the same air kerma. At field sizes between 60 cm × 60 cm and 100 cm × 100 cm, the simulated value for this ratio ranged from 67(2)% to 77(2)%. More accurate simulations should implement beams diverging from an actual source contained in actual housing, rather than flat and parallel beams originating free in air. Such simulations would be able to evaluate more closely the response of the modelled nanoDots in comparison with the response of actual nanoDots. For reference, a more sophisticated nanoDot model exists in the literature [19]. It is also worth noting that the current work models the active detector disks as homogenous. Any role that the internal structure of the Al<sub>2</sub>O<sub>3</sub> powder and binder in the disks could play has therefore not been investigated.

It is impossible to compare values for the simulated specific energy imparted to nanoDots to the measured read doses without knowing the buildup conditions employed at the Landauer calibration facility. The fact that the measured dose in the Cs-137 beam relatively closely matches the air kerma in air at the location of the nanoDots, however indicates that buildup conditions probably were similar between the Landauer calibration facility and the exposures at the SSDL at the NRPA. The simulations also indicate that the exposures at the SSDL at the NRPA in the Cs-137 beam at a distance of 2.0 m from the source focus where the field diameter was about 44 cm likely provided close to full buildup from electrons liberated in air. If

---

both these assumptions are correct, then the calibration nanoDots experienced close to full buildup from air in the exposures at the Landauer calibration facility.

## **6 Recommendations and outlook**

### **6.1 Buildup for air kerma in air measurements with nanoDots**

The current work demonstrates that nanoDots exposed free in air without buildup in Cs-137 and Co-60 beams can receive a substantial signal originating from secondary electrons liberated in air or in the materials of the source and source housing. Air kerma measurements in air with Landauer nanoDots should therefore be conducted with beam energy appropriate buildup, both in Cs-137 and definitely in Co-60 beams so that the signal on the nanoDots originates solely from electrons that were liberated either in the buildup or in the materials of the detectors themselves. This applies also to air kerma in air calibration exposures.

# 7 Appendix

## 7.1 Cs-137 air kerma in air calibration certificate purchased from Landauer

Exposure Request#	Req. Kerma mrad	Date Completed	SERIAL #	Source	Phantom	Angle	Axis	Holder	Delivered Exposure			Pressure mm Hg	Exp Time (min)	Lab Tech
									DDE mrem	SDE mrem	Kerma mrad			
42073_36612	0	03/12/2015	DN08257769B	Unirradiated	Air	0	Hor	None	0	0	0	758	0	CS
42073_36612	0	03/12/2015	DN08258018V	Unirradiated	Air	0	Hor	None	0	0	0	758	0	CS
42073_36612	0	03/12/2015	DN082732140	Unirradiated	Air	0	Hor	None	0	0	0	758	0	CS
42073_36613	500	03/12/2015	DN08517527S	Cs137 Pan	Air	0	Hor	None	492	492	492	758	5.71	CS
42073_36613	500	03/12/2015	DN08850414X	Cs137 Pan	Air	0	Hor	None	492	492	492	758	5.71	CS
42073_36613	500	03/12/2015	DN106064768	Cs137 Pan	Air	0	Hor	None	492	492	492	758	5.71	CS
42073_36546	3,000	03/12/2015	DN08517535V	Cs137 Pan	Air	0	Hor	None	3,001	3,001	3,001	758	3.17	CS
42073_36546	3,000	03/12/2015	DN08850416T	Cs137 Pan	Air	0	Hor	None	3,001	3,001	3,001	758	3.17	CS
42073_36546	3,000	03/12/2015	DN08850419N	Cs137 Pan	Air	0	Hor	None	3,001	3,001	3,001	758	3.17	CS
42073_36298	50,000	03/12/2015	DN088504030	Cs137 Pan	Air	0	Hor	None	49,967	49,967	49,967	758	52.82	CS
42073_36298	50,000	03/12/2015	DN08850418P	Cs137 Pan	Air	0	Hor	None	49,967	49,967	49,967	758	52.82	CS
42073_36298	50,000	03/12/2015	DN10408482F	Cs137 Pan	Air	0	Hor	None	49,967	49,967	49,967	758	52.82	CS
42073_36348	100,000	03/12/2015	DN086181921	Cs137 Pan	Air	0	Hor	None	99,902	99,902	99,902	758	105.63	CS
42073_36348	100,000	03/12/2015	DN086182119	Cs137 Pan	Air	0	Hor	None	99,902	99,902	99,902	758	105.63	CS
42073_36348	100,000	03/12/2015	DN086182309	Cs137 Pan	Air	0	Hor	None	99,902	99,902	99,902	758	105.63	CS



# Landauer Irradiation Certificate



Customer Contact: Landauer Inlight  
 Customer Address: 2 Science Road Glenwood, IL 60425  
 Exposure Description: Calibrate Set

This calibration is directly traceable to the National Institute of Standards and Technology (NIST) and the University of Wisconsin via air ionization chambers A3-111, A5-234 or A3-160. The expanded uncertainty of 5% is the standard uncertainty of measurement multiplied by the coverage factor k=2, which for a normal distribution corresponds to a coverage probability of approximately 95%.

Approved: *[Signature]*

Laboratory Manager  
 Report Number: 20150316 -1125

---

## 7.2 Exposures of nanoDots with beam energy appropriate buildup at FIGARO for the DoReMi CloGiGat project

During the DoReMi CloGiGat project concerning the chronic exposure of mice at the FIGARO Co-60 irradiation facility, nanoDot detectors and the microStar reader were used for the dosimetry. The nanoDots were exposed with PMMA buildup on mice cages in an air flow IVC rack (Innovive Inc., San Diego, CA) for 159.6 h, starting 18/02/2015 and ending 25/02/2015, at a distance to the center of the central cage from the source focus of 650 cm. Measurements by the SSDL at the NRPA predict an air kerma rate free in air at this distance between 18/02/2015 and 22/02/2015 of 2.50 mGy/h with a combined relative standard uncertainty of 4% [20]. The background corrected measured dose read on nanoDots in this time interval gave an air kerma rate in the center of the central cage of 2.53 mGy/h with a combined relative standard uncertainty of 7%, in excellent agreement with the SSDL measurements. The measurements agree with the hypothesis that the dose measured with beam energy appropriate buildup in a Co-60 beam using the Landauer calibration certificate (see appendix) is the air kerma rate free in air.

## 8 Acknowledgements

This work was partly supported by the Research Council of Norway through its Centers of Excellence funding scheme, project number 223268/F50 and partly supported by the Research Council of Norway, contract number 217334 (DoReMi). Elisabeth thanks Lene Valle, Yetneberk Ayalew Kassaye, Dag Anders Brede and Ole Christian Lind for discussions and help at FIGARO and Hans Bjerke from the SSDL at the NRPA for helpful comments. Data analysis in the current work was done in tidyverse [21] R [22].

---

## 9 References

1. BIMP, Calibration certificate for Exradin A6 (serial nr. XQ102232). (2013).
2. BIMP, Calibration certificate for Capintec PR-06G (serial nr. 8429). (2013).
3. S. Agostinelli, et al., Geant4 - a simulation toolkit. Nucl. Instr. Meth. Phys. Res. A 506 (3), 250 (2003).
4. J. Allison, et al., Geant4 developments and applications. {IEEE} Trans. Nucl. Sci. 53 (1), 270 (2006).
5. S. Incerti, et al., Comparison of GEANT4 very low energy cross section models with experimental data in water. Med. Phys. 37 (9), 4692 (2010).
6. J.H. Hubbell and S.M. Seltzer, Tables of X-Ray Mass Attenuation Coefficients and Mass Energy-Absorption Coefficients (version 1.4), National Institute of Standards and Technology: Gaithersburg, MD (2004).
7. ICRU, ICRU Report 85: Fundamental Quantities and Units for Ionizing Radiation. Journal of the ICRU 11 (1), (2011).
8. P. Andreo, J.P. Seuntjens, and E.B. Podgorsak, Calibration of Photon and Electron Beams, in Review of Radiation Oncology Physics: A Handbook for Teachers and Students, E.B. Podgorsak, Editor., IAEA: Vienna, Austria (2003).
9. M.J. Berger, J.H. Hubbell, S.M. Seltzer, J. Chang, J.S. Coursey, R. Sukumar, D.S. Zucker, and K. Olsen, XCOM: Photon Cross Section Database (version 1.5). [cited 16/06/2015], <http://www.nist.gov/pml/data/xcom/index.cfm>
10. M.J. Berger, J.S. Coursey, M.A. Zucker, and J. Chang, ESTAR, PSTAR, and ASTAR: Computer Programs for Calculating Stopping-Power and Range Tables for Electrons, Protons, and Helium Ions (version 1.2.3). [cited 08/06/2015], <http://www.nist.gov/pml/data/star/index.cfm>
11. J. Lilley, Nuclear Physics: Principles and Applications. The Manchester Physics Series, ed. D.J. Sandiford, et al., Norfolk, Great Britain: John Wiley & Sons, Ltd. (2006).
12. J.P. Seuntjens, W. Strydom, and K.R. Shortt, Dosimetric Principles, Quantities and Units, in Review of Radiation Oncology Physics: A Handbook for Teachers and Students, E.B. Podgorsak, Editor., IAEA: Vienna, Austria (2003).
13. C. Rose and M.D. Smith, Mathematical Statistics with Mathematica. Springer Texts in Statistics. New York: Springer-Verlag (2002).
14. J.L. Devore and K.N. Berk, Modern Mathematical Statistics with Applications. 2nd ed. Springer Texts in Statistics, ed. G. Casella, et al., New York: Springer-Verlag (2012).
15. BIPM, IEC, IFCC, ILAC, ISO, IUPAC, IUPAP, and OIML, Evaluation of measurement data - Guide to the expression of uncertainty in measurement (GUM 1995 with minor corrections), in JCGM 100 (2008).
16. P.A. Jursinic, Characterization of optically stimulated luminescent dosimeters, OSLDs, for clinical dosimetric measurements. Med Phys 34 (12), 4594 (2007).
17. S.B. Scarboro, D. Cody, P. Alvarez, D. Followill, L. Court, F.C. Stingo, D. Zhang, M. McNitt-Gray, and S.F. Kry, Characterization of the nanoDot OSLD dosimeter in CT. Med Phys 42 (4), 1797 (2015).
18. J.R. Kerns, S.F. Kry, N. Sahoo, D.S. Followill, and G.S. Ibbott, Angular dependence of the nanoDot OSL dosimeter. Med Phys 38 (7), 3955 (2011).
19. J. Lehmann, L. Dunn, J.E. Lye, J.W. Kenny, A.D.C. Alves, A. Cole, A. Asena, T. Kron, and I.M. Williams, Angular dependence of the response of the nanoDot OSLD system for measurements at depth in clinical megavoltage beams. Medical Physics 41 (6), 061712 (2014).

- 
20. H. Bjerke and P.O. Hetland, Dosimetri ved FIGARO gammaanlegget ved NMBU, Ås. Målerapport fra oppmåling av doseraten i strålefeltet fra kobolt-60. NRPA Technical Document Series 2 (2014).
  21. H. Wickham, tidyverse: Easily Install and Load 'Tidyverse' Packages. R package version 1.0.0., (2016).
  22. R.C. Team, R: A language and environment for statistical computing, R Foundation for Statistical Computing: Vienna, Austria (2016).



Statens strålevern  
Norwegian Radiation Protection Authority